Available online at www.sciencedirect.com
SCIENCE DIRECT®
Journal of Catalysis 225 (2004) 428–438
JOURNAL OF CATALYSIS
www.elsevier.com/locate/jcat

Selective oxidative dehydrogenation of ethane on MoVTeNbO mixed metal oxide catalysts

P. Botella,[a] E. García-González,[b] A. Dejoz,[c] J.M. López Nieto,[a,*] M.I. Vázquez,[c] and J. González-Calbet[b]

[a] *Instituto de Tecnología Química, UPV-CSIC, Avda. Los Naranjos s/n, 46022 Valencia, Spain*
[b] *Departamento Química Inorgánica, Facultad de Ciencias Químicas, Universidad Complutense Madrid, 28040 Madrid, Spain*
[c] *Departamento de Ingeniería Química, Universidad de Valencia, Dr. Moliner 50, 46100 Burjassot, Spain*

Received 23 January 2004; revised 29 March 2004; accepted 20 April 2004

Available online 28 May 2004

Abstract

MoVTeNbO catalysts, prepared by hydrothermal synthesis, are active and highly selective in the ODH of ethane, especially those with a Mo–V–Te–Nb molar ratio of 1–0.15–0.16–0.17 and heat-treated at 600–650 °C. On the best catalyst, selectivities higher than 80% at ethane conversion levels higher than 80% have been obtained operating at relatively low reaction temperatures (340–400 °C). Thus, yields of ethylene of ca. 75% have been obtained, which exceeds the best yield reported in the literature. $Te_2M_{20}O_{57}$ (M = Mo, V, Nb) and (V,Nb)-substituted θ-Mo_5O_{14}, in addition to small amounts of the $Te_{0.33}MO_{3.33}$ (M = Mo, V, Nb) phase, can be proposed in the most selective catalysts from XRD, SAED, and HREM results. However, the catalytic performance in ethane oxidation can mainly be related to the presence of the multifunctional $Te_2M_{20}O_{57}$ orthorhombic phase in cooperation with the Mo_5O_{14}-type phase. The nature of active and selective sites is discussed.

Keywords: Selective oxidation of ethane to ethylene; Mo–V–Te–Nb mixed metal oxide catalyst; Hydrothermal synthesis; Catalyst characterization; X-ray diffraction; SEM-EDX; SAED; HREM; XPS

1. Introduction

Over the past two decades, research efforts in both academy and industrial laboratories have been devoted to the conversion of light alkanes to olefins and/or the substitution of olefins by paraffins in well-developed industrial processes [1–7]. The oxidative dehydrogenation (ODH) of short chain alkanes is an interesting alternative way for olefin production [4–7], since it is thermodynamically favored, and it can be carried out at lower reaction temperatures without coke formation.

Several catalytic systems have been proposed in the last decade, although the reaction conditions and the mechanism involved strongly depend on the catalytic systems [4–17]. Nonreducible catalysts (i.e., alkaline earth metal-based oxides Li/MgO-type and related materials) present high selectivities and yields of ethylene, but they operate at reaction temperatures higher than 600 °C [4,5,8]. In this case, the catalyst is only involved in the heterolytic scission of a C–H bond forming the ethyl radical.

A great variety of reducible metal oxide-based catalysts have been tested in the last years [1–7,9–17], some of them developed from combinatorial heterogeneous catalysis [14–17]. They generally work at reaction temperatures below 600 °C and operate according to a redox (Mars–van Krevelen) mechanism. Within all of them, those containing vanadium, i.e., vanadium mixed metal oxides, vanadia supported on metal oxides, or V-containing microporous/mesoporous materials [1–7,9], seem to be the most promising catalytic systems. This is the case of Mo–V–Nb–O mixed metal oxide catalysts, which can operate at reaction temperatures lower than 450 °C with relatively high efficiencies [10–14]. The incorporation of metal oxide promoters allows a clear enhancement of its catalytic performance [18,19]. Thus, the patent literature presents

* Corresponding author. Fax: 0034-96-3877809.
E-mail address: jmlopez@itq.upv.es (J.M. López Nieto).

0021-9517/$ – see front matter
doi:10.1016/j.jcat.2004.04.024

Sb-promoted Mo–V–Nb mixed oxides, which show ethane conversions of 73% with selectivity to ethylene of 71% [19].

Recently, it has been reported that MoVTeNbO mixed metal oxide catalysts are active and selective in the ODH of ethane [20,21]. The catalyst, prepared by hydrothermal synthesis and heat-treated in N_2 at high temperature, presents yields of ethylene about 75% [20], while Te-doped MoVNbO catalysts present yields of ca. 12% [22].

In this paper, we report the catalytic performance of Mo–V–Te–Nb oxide, prepared by hydrothermal synthesis, with different compositions. We will show that these catalysts are very active and selective in the oxidative dehydrogenation of ethane to ethylene, although the chemical composition and the calcination temperature can modify both activity and selectivity. In addition, the nature of active and selective sites for the oxidative dehydrogenation of ethane is tentatively proposed.

2. Experimental

2.1. Catalyst preparation

Mo–V–Te–Nb–O catalysts have been prepared hydrothermally from aqueous gels of vanadyl sulfate, niobium oxalate, ammonium heptamolybdate, and telluric acid [23]. The gels were autoclaved in Teflon-lined stainless-steel autoclaves at 175 °C for 60 h. The resulting precursors were filtered, washed, dried at 80 °C for 16 h, and heat-treated. Finally, the samples were generally heat-treated in N_2 at 600 (samples HT-1 to HT-8) or 650 °C (sample HT-4-B) for 2 h. The characteristics of catalysts are shown in Table 1.

2.2. Catalyst characterization

Powder X-ray diffraction patterns (XRD) were collected using a Philips X'Pert diffractometer equipped with a graphite monochromator, operating at 40 kV and 45 mA and employing nickel-filtered Cu-Kα radiation ($\lambda = 0.1542$ nm).

The chemical composition was determined by EDS X-ray microanalysis carried out on both a JEOL 2000FX electron microscope supplied with a LINK analyser AN10000 and a PHILIPS CM20FEG Super Twin electron microscope supplied with an EDAX analyser DX-4 (resolution ≈ 135 eV and Super Ultra Thin Window).

Selected area electron diffraction (SAED) was carried out on a JEOL 2000FX electron microscope. High-resolution electron microscopy (HREM) was performed on a PHILIPS CM20FEG Super Twin electron microscope. The samples for electron microscopy were ultrasonically dispersed in *n*-butanol and transferred to carbon-coated copper grids.

Photoelectron spectra (XPS) were recorded on a VG-Escalab-210 electron spectrometer using Mg-Kα radiation (EMg-K$\alpha = 1253.6$ eV) of a twin anode in the constant analyzer energy mode, with a pass energy of 50 eV. Samples were previously outgassed at 100 °C for 2 h in the preparation chamber of the spectrometer and subsequently transferred to the analysis chamber. The pressure of the main chamber was maintained at ca. 5×10^{-10} mb. The binding energy (BE) scale was regulated by setting the C_{1s} transition at 284.6 eV. The accuracy of the BE was ± 0.1 eV.

2.3. Catalytic tests

The catalytic experiments were carried out under steady-state conditions using a fixed-bed quartz tubular reactor (i.d. 20 mm, length 400 mm), equipped with a coaxial thermocouple for catalytic bed temperature profiling, working at atmospheric pressure. The flow rate (25–100 ml min^{-1}) and the amount of catalyst (0.5–2.0 g, 0.3–0.5 mm particle size) were varied in order to achieve different ethane conversion levels. The feed consisted of a mixture of ethane/oxygen/helium with molar ratios of 9/6/85 or $30/x/70-x$ ($x = 10$–30). Experiments were carried out in the 325 to 425 °C temperature range. Reactants and reaction products were analyzed by on-line gas chromatography, using two columns:

(i) Porapak QS (2.0 m $\times$ 1/8 in) to separate hydrocarbons and CO_2 and partial oxidation products;
(ii) Carbosieve-S (2.5 m $\times$ 1/8 in) to separate O_2 and CO [14].

Blank run experiments have been carried out at the lowest total flow used (25 ml min^{-1}) with an ethane/oxygen/helium molar ratio of $30/x/70-x$ ($x = 10$–30) and using an inert material (SiC) instead of the catalyst. No ethane conversion was observed at 400 °C, and a conversion of ethane of 0.14% was only observed at 500 °C. So, the presence of homogeneous reaction can be neglected.

3. Results

3.1. Oxidative dehydrogenation of ethane

The catalytic results for the oxidative dehydrogenation of ethane on MoVNb-based catalysts, prepared by hydrothermal synthesis and heat-treated at 600–650 °C, are presented in Table 2. Ethylene, CO, and CO_2 were the main reaction products. Oxygenated products other than carbon oxides (CO and CO_2) were not observed.

According to the results of Table 2, high selectivities to ethylene are achieved on MoVTeNbO catalysts. In this way, a space–time yield (STY) of ethylene of ca. 275 $g_{C_2H_4}$ kg_{cat}^{-1} h^{-1} has been obtained at 380 °C and a C_2H_6/O_2/He molar ratio of 30/10/60 on the most active catalyst. However, the catalytic performance of these catalysts strongly depends on both the V/Mo ratio of synthesis gel and the catalyst composition.

Sample HT-1, without vanadium, is practically inactive in the ODH of ethane to ethylene, while V-containing sam-

Table 1
Characteristics of MoVTeNbO catalysts

Sample	S_{BET} ($m^2\ g^{-1}$)	Mo–V–Te–Nb ratio		
		Gel composition[a]	Bulk composition[b]	XPS composition[c]
HT-1	1.0	1–0.0–0.17–0.12	1–0.0–0.69–0.86	1–0.0–0.45–0.51
HT-2	nd	1–0.12–0.17–0.17	1–0.08–0.17–0.17	nd
HT-3	nd	1–0.20–0.17–0.08	1–0.14–0.18–0.07	nd
HT-4	9.1	1–0.20–0.17–0.17	1–0.14–0.19–0.17	1–0.11–0.19–0.22
HT-4-B	4.0	1–0.20–0.17–0.17	1–0.15–0.16–0.17	nd
HT-5	11.8	1–0.40–0.17–0.17	1–0.39–0.16–0.17	1–0.31–0.16–0.10
HT-6	nd	1–0.60–0.17–0.17	1–0.24–0.15–0.19	nd
HT-7	nd	1–0.20–0.17–0.34	1–0.14–0.25–0.42	nd
HT-8	20.8	1–0.22–0.0–0.17	1–0.10–0.0–0.21	nd

[a] Gel composition as determined by atomic absorption spectroscopy.
[b] Chemical composition of heat-treated samples as determined by atomic absorption spectroscopy.
[c] XPS of heat-treated samples.

Table 2
ODH of ethane on Te-containing catalysts[a]

Sample	Temperature (°C)	Conversion (%)	Selectivity (%)			$STY_{C_2H_4}$[b]
			C_2H_4	CO	CO_2	
HT-1	420	0.2	10.3	10.0	79.7	0.1
HT-2	340	2.1	97.6	1.0	1.4	15.1
	380	6.3	95.9	2.5	1.6	44.5
HT-3	340	14.5	96.6	2.1	1.3	103
	380	28.2	92.1	4.6	3.3	191
HT-4	340	10.3	96.9	1.9	1.2	73.5
	380	29.0	94.5	3.4	2.2	202
HT-4-B	340	19.7	97.1	1.7	1.2	141
	380	36.5	96.3	2.2	1.5	259
HT-5	340	20.2	97.1	1.9	1.0	145
	380	39.8	93.9	3.8	2.3	275
HT-6	340	4.3	95.4	2.4	2.2	30.2
	380	12.5	94.5	3.4	2.1	87.0
HT-7	340	1.5	84.2	4.1	11.7	9.3
	380	4.0	87.4	5.5	7.1	25.8
HT-8	340	1.8	78.9	13.2	7.8	10.2
	380	5.6	75.8	17.1	7.1	31.3

[a] Ethane/O_2/He molar ratio of 30/10/60; contact time, W/F, of 38.0 $g_{cat}\ h\ mol^{-1}_{C_2H_6}$.
[b] Rate formation of ethylene per unit mass of catalyst, $STY_{C_2H_4}$ (space–time yield), in $g_{C_2H_4}\ kg^{-1}_{cat}\ h^{-1}$.

ples are active in ethane conversion. On the other hand, Te-containing samples (HT-2 to HT-7) show high selectivities to ethylene at high ethane conversions, whereas the Te-free sample (HT-8) shows relatively low selectivity to ethylene.

Fig. 1 presents the variation of the ethane conversion and the space–time yield of ethylene with the V/Mo atomic ratio in the synthesis gel (Fig. 1a) or in the catalysts (Fig. 1b). Both the catalytic activity and the formation rate of ethylene per unit mass of catalyst ($STY_{C_2H_4}$) increase initially with the V content, presenting a maximum for a V/Mo atomic ratio of ca. 0.4 (Fig. 1a). However, the catalytic activity strongly decreases on the catalyst prepared from synthesis gels with V/Mo atomic ratios higher than 0.4.

If we compare the V/Mo atomic ratio in the synthesis gels with those obtained in the corresponding heat-treated samples (Table 1) it can be concluded that a poor incorporation

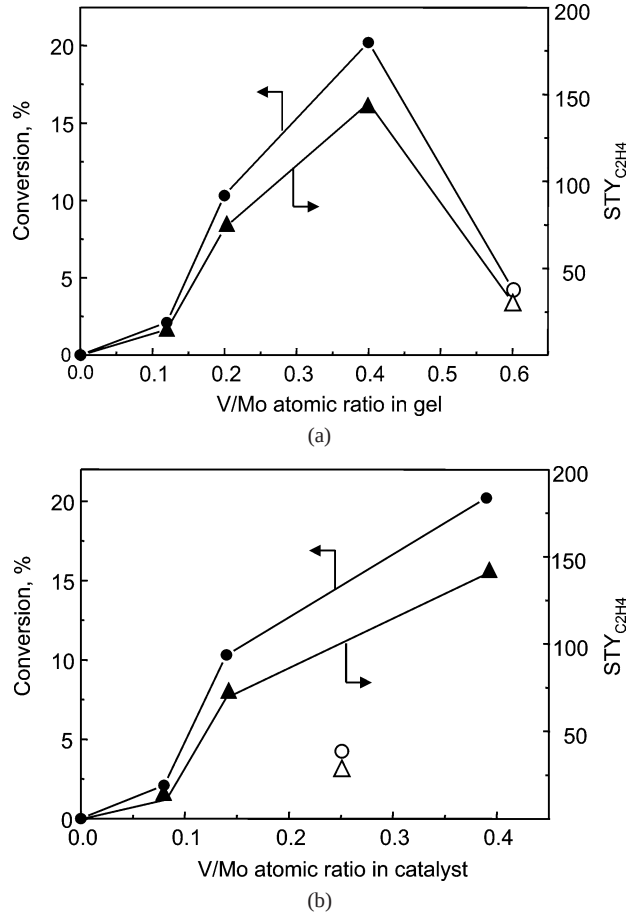

Fig. 1. Variation of the ethane conversion (●) and the space–time yield of ethylene per unit mass of catalyst per unit time, $STY_{C_2H_4}$ (in $g_{C_2H_4}\ kg^{-1}_{cat}\ h^{-1}$), (▲) with the V/Mo atomic ratio of the synthesis gel (a) or the V/Mo atomic ratio of catalysts (b) obtained during the oxidation of ethane at 340 °C on MoVTeNbO catalysts. For comparison the catalytic results of sample HT-6 (○,△) have also been included.

of vanadium occurs in catalysts prepared with high V/Mo ratios in the synthesis gel (sample HT-6). However, the results presented in Fig. 1b suggest a linear correlation between catalytic activity and ethylene formation with the V/Mo ratio in the catalyst, except in the sample HT-6 which presents

a lower catalytic activity than the corresponding sample prepared with a lower V/Mo ratio in the synthesis gel. According to these results, V sites can be proposed as the active sites in the oxidative activation of ethane, although a linear correlation between ethane reactivity (or ethylene formation) and vanadium content cannot directly be concluded from the results of Fig. 1b. As it will be discussed below, the results obtained could be explained by considering different types of V sites in these catalysts [23] as a consequence of the formation of different crystalline phases [23–26].

Figs. 2 and 3 present the variation of the selectivity to the main reaction products with the ethane conversion obtained on catalysts with different compositions. Small differences in the selectivity to ethylene are observed at low ethane conversions on MoVTeNbO catalysts. In this way, it can be noted that selectivities to ethylene higher than 90% were obtained on the main Te-containing catalysts, while the Te-free sample showed the lowest value.

On the other hand, the selectivity to ethylene slowly decreases and the selectivity to CO and/or CO_2 increases at high ethane conversions. According to these results, the following reaction network can be proposed:

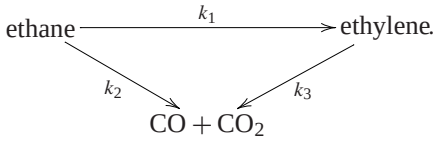

Ethylene is the most abundant primary product during the oxidation of ethane on Mo–V–Te–Nb–O catalysts, while CO and CO_2 come from the deep oxidation of both the alkane and the corresponding olefin. This reaction network has also been reported on previous vanadium-containing catalysts [5–7,9–14]. However, the relatively deep oxidation of ethane and ethylene strongly depends on the catalyst composition. Te-free catalysts present not only the lowest selectivity to ethylene at low ethane conversion levels but the highest deep oxidation of ethylene at high ethane conversions, then presenting the lowest k_1/k_2 and k_1/k_3 ratios. However, the highest selectivities to ethylene (and also the highest k_1/k_2 and k_1/k_3 ratios) correspond to samples HT-4, HT-5, and HT-4-B.

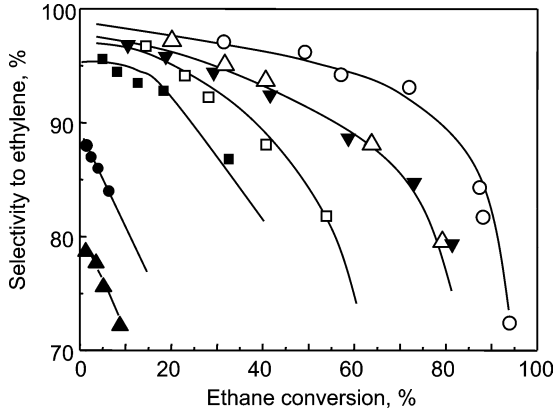

Fig. 2. Variation of the selectivity to ethylene with the ethane conversion obtained during the oxidation of ethane on Te-free and Te-containing catalysts: HT-2 (■); HT-3 (□); HT-4 (△); HT-4-B (○); HT-5 (▼); HT-7 (●); HT-8 (▲).

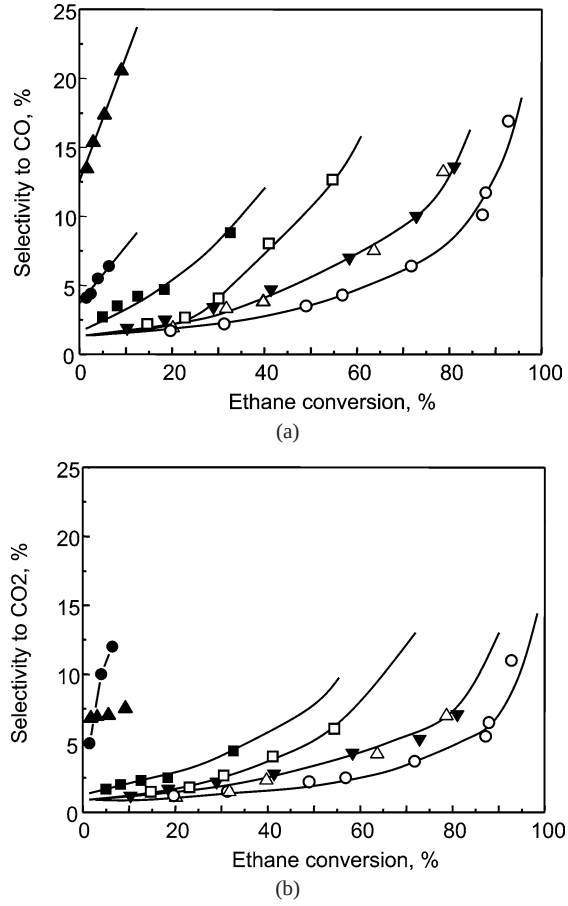

Fig. 3. Variation of the selectivity to CO (a) and CO_2 (b) with the ethane conversion obtained during the oxidation of ethane on Te-free and Te-containing catalysts: HT-2 (■); HT-3 (□); HT-4 (△); HT-4-B (○); HT-5 (▼); HT-7 (●); HT-8 (▲).

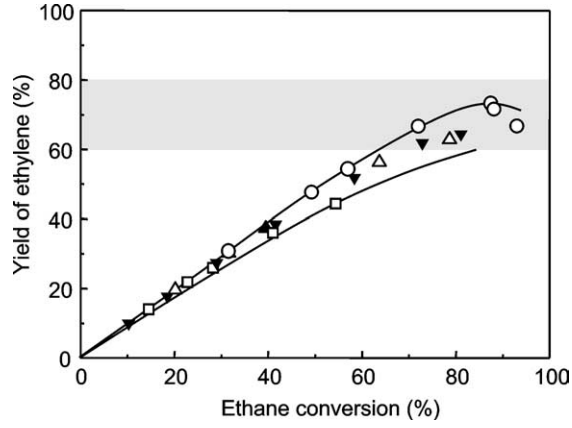

Fig. 4. Variation of the yield of ethylene with the ethane conversion obtained during the oxidation of ethane on Mo–V–Nb–Te catalysts: HT-3 (□); HT-4 (△); HT-4-B (○); HT-5 (▼).

Fig. 4 shows the variation of the yield of ethylene with the ethane conversion under different reaction conditions on the

Table 3
Catalytic performance during the ethane oxidation at 400 °C on HT-4-B catalyst

C_2H_6/O_2/He molar ratio	W/F[a]	Conversion (%)	Selectivity (%)			$STY_{C_2H_4}$[b]
			C_2H_4	CO	CO_2	
30–10–60	87	48.8[c]	88.8	6.9	4.3	139.5
30–20–50	87	59.4	89.3	7.0	3.7	170.7
30–20–50	174	70.1[c]	80.3	12.0	5.3	91.1
30–30–40	174	80.9	79.2	13.6	7.7	103.7
9–6–85	238	87.2	84.4	10.1	5.5	86.6

[a] Contact time, W/F, in $g_{cat}\,h\,mol^{-1}_{C_2H_6}$.

[b] Rate formation of ethylene per unit mass of catalyst, $STY_{C_2H_4}$ (space–time yield), in $g_{C_2H_4}\,kg^{-1}_{cat}\,h^{-1}$.

[c] Total oxygen consumption has been observed.

best catalysts. Yields of ethylene of 60 to 75% have been achieved at ethane conversions higher than 80% on catalysts with Mo/V/Te/Nb atomic ratios of 1/0.14–0.39/0.18–0.25/0.17–0.19.

Table 3 presents the catalytic results obtained on sample HT-4-B by using different C_2H_6/O_2 ratios. Total O_2 consumption can be achieved by working at high C_2H_6/O_2 ratios and high ethane conversion levels. Therefore, the C_2H_6/O_2 ratio should be optimized depending on the ethane conversion to be reached, although lower C_2H_6/O_2 molar ratios should be used in order to obtain high ethane conversions. In this way, the best catalytic results were obtained on sample HT-4-B, which presents a selectivity to ethylene of ca. 84.4% at a ethane conversion of 87.2%, working with a C_2H_4/O_2/He molar ratio of 9/6/85 and a contact time, W/F, of 238 $g_{cat}\,h\,mol^{-1}_{C_2H_6}$. These results represent a yield of ethylene of ca. 75% and a space–time yield, $STY_{C_2H_4}$, of 86.6 $g_{C_2H_4}\,kg^{-1}_{cat}\,h^{-1}$ at 400 °C. This yield of ethylene is higher than those previously reported by Union Carbide researchers on undoped [10,18] and Sb-doped MoVNbO [19] catalysts.

From an industrial point of view, it has been proposed that ethylene yields between 65 and 70% are required to compete with the steam-cracking process [17]. According to our results, the oxidative dehydrogenation of ethane on MoVTeNbO catalysts could be a competitive alternative to the actual industrial process in ethylene production.

3.2. Catalyst characterization

Table 1 shows the characteristics of catalysts. Low surface areas have been obtained in all cases. On the other hand, the chemical composition of calcined samples strongly depends on the composition of the gel. As a general trend, the higher the vanadium or the niobium contents in the synthesis gel the higher the amounts of these elements in the calcined samples. However, a V/Mo ratio of about 0.4 was the highest incorporation of vanadium in our catalysts. Therefore, the preparation conditions seem to have a strong influence of the incorporation of each element in the solid during the hydrothermal synthesis. On the other hand, no apparent influence of the V or Nb content on the incorporation of other elements can be proposed.

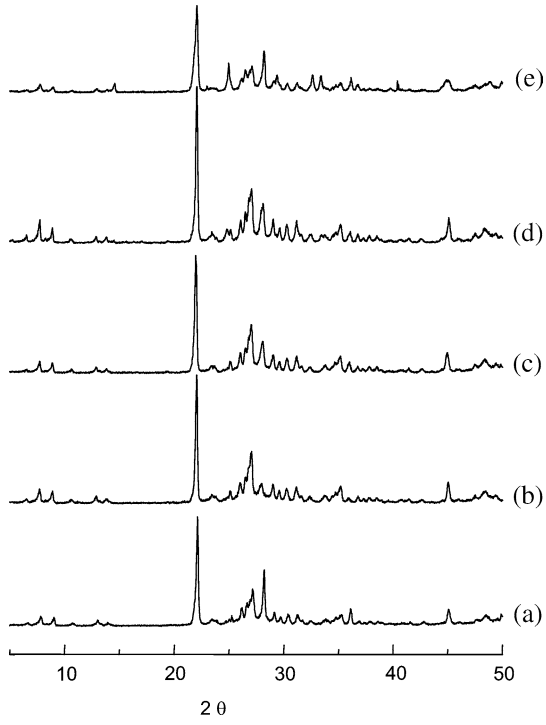

Fig. 5. XRD patterns of catalysts: HT-3 (a); HT-4 (b); HT-4-B (c); HT-5 (d); HT-6 (e).

Fig. 5 shows the XRD patterns of samples prepared by hydrothermal synthesis. The XRD pattern of the sample without vanadium, i.e., sample HT-1 (pattern not shown), suggested the presence of $Nb_{0.09}Mo_{0.91}O_{2.80}$ and $3MoO_2$-Nb_2O_5 [23]. However, no Te-containing crystalline phases were observed. On the other hand, the sample without tellurium, i.e., HT-8 (pattern not shown), suggested the presence of $(V_{0.07}Mo_{0.93})_5O_{14}$ and/or $(Nb_{0.09}Mo_{0.91})O_{2.80}$ and small amounts of MoO_2 [14].

The XRD patterns obtained for the V-containing MoTeNbO catalysts show diffraction maxima at $2\theta(^\circ) = 7.6$, 8.6, 12.2, 13.8, 16.4, 22.1, 23.5, 24.8, 26.3, 26.6, 26.9, 28.3, 30.5, 31.4, 34.8, and 45.0 (Fig. 5, diffractograms (b)–(e)). Although they are rather complex, the presence of $(V_{0.07}Mo_{0.93})_5O_{14}$ and/or $(Nb_{0.09}Mo_{0.91})O_{2.80}$, $Te_{0.33}MO_{3.33}$ (M = Mo, V, Nb) and $TeMo_5O_{16}$ has been suggested in addition to a new Te-containing phase [23], which could be associated with the orthorhombic $Te_2M_{20}O_{57}$ (M = Mo, V, and Nb) [24–26].

In the case of samples prepared with high V/Mo atomic ratios in the synthesis gel (i.e., sample HT-6), the corresponding diffraction pattern is similar to that observed for samples with lower V contents, although the maxima related to the $Te_{0.33}MO_{3.33}$ phase (i.e., at $2\theta(^\circ) = 22.1$, 28.2, 36.2, 45.2, and 50.0) show higher intensities (Fig. 5e). Therefore, the incorporation of higher amounts of vanadium in the synthesis gel could favor the formation of $Te_{0.33}MO_{3.33}$ phase, while the use of gels with a V/Mo atomic ratio of 0.2–0.4 could favor the formation of $Te_2M_{20}O_{57}$.

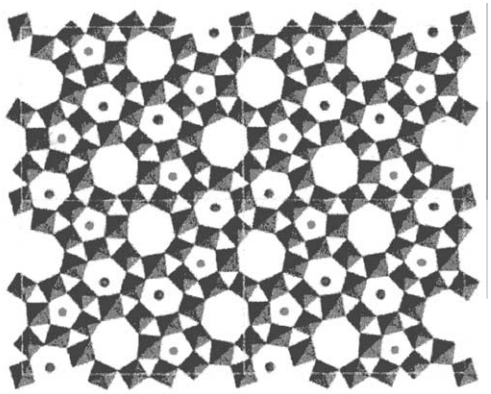

(a)

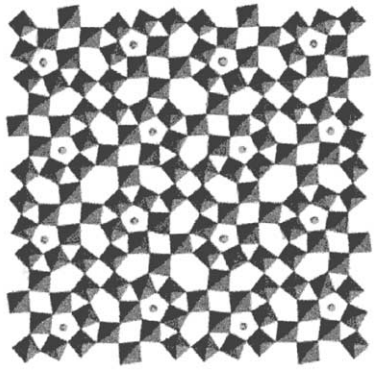

(b)

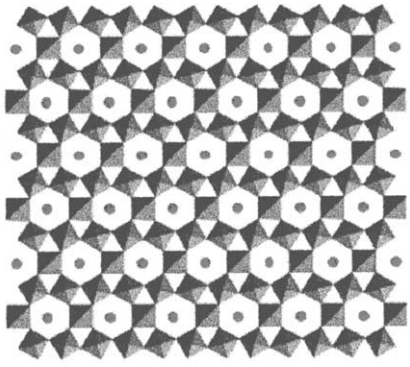

(c)

Fig. 6. Model structures of $Te_2M_{20}O_{57}$ (a), Mo_5O_{14} (b), and $Te_{0.33}MO_{3.33}$ (c) crystalline phases.

Provided the structural similarities for some of the constituent crystalline phases, there are several diffraction maxima which are coincident, and estimation of their relative amounts cannot be made with acceptable precision. For this reason, the nature of the different crystalline phases in MoVTeNbO catalysts has been further analyzed in detail by electron microscopy. The careful observation of the samples allowed us to show that the multicomponent catalyst is constituted by the so-called $Te_2M_{20}O_{57}$ (M = Mo, V, and Nb) phase as the main component; crystals of the $Mo_{5-x}(V,Nb)_xO_{14}$ type phase are also found, this phase being considered as the second one in abundance in this material. Finally, a small amount of the $Te_{0.33}MO_{3.33}$ (M = Mo, V, and Nb) phase was found to be the third component of this multiphase catalyst.

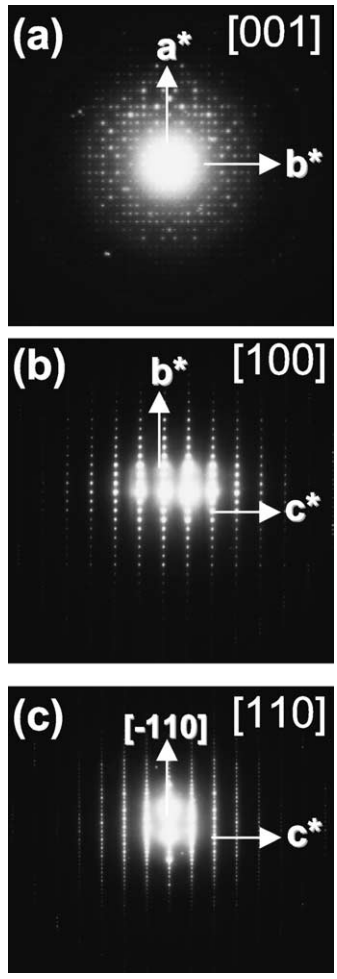

Fig. 7. SAED patterns of $Te_2M_{20}O_{57}$ crystal taken along [001] (a), [010] (b), and [110] (c) zone axes.

The $Te_2M_{20}O_{57}$ phase, isostructural with $Cs_x(Nb,W)_5O_{14}$ [27], presents orthorhombic symmetry ($a = 2.71$, $b = 2.16$, $c = 0.39$ nm) and exhibits a quite complex network of MO_6 octahedra forming hexagonal channels as well as pentagonal and heptagonal ones (Fig. 6a). The pentagonal channels are occupied by M cations, forming MO_7 pentagonal bipyramidal groups. Tellurium atoms are located in the hexagonal channels, which are fully occupied for a Te/M ratio equal to 0.1. Higher Te/M ratios would imply location of the extra tellurium atoms inside the heptagonal tunnels.

The chemical analysis of the crystals has been performed by means of EDS X-ray microanalysis. The Te/M atomic ratio (M = Mo + V + Nb) was found to change in the range 0.10–0.12 (± 0.01) in all the $Te_2M_{20}O_{57}$-like crystals investigated. An increasing/decreasing tellurium quantity does only originate a lower average oxidation state, which is related to a modulated Mo/Nb ratio. However, independently of the tellurium amount, crystals show always a vanadium content close to 10% of the M positions of the skeleton. These results would lead to the av-

erage composition $Te_{0.57}(Mo_{0.72}Nb_{0.13}V_{0.14})_5O_{14}$ based on the $Te_2M_{20}O_{57}$ phase stoichiometry.

Fig. 7a shows the selected area electron diffraction pattern (SAED) along the [001] zone axis. The diagram identifies the phase unit cell parameters $a \approx 2.7$ nm and $b \approx 2.1$ nm. Fig. 7b and 7c correspond to the [010] and [110] reciprocal lattice projections, respectively. The reconstruction of the three-dimensional reciprocal lattice was used to confirm the crystal structure. The metric of the unit cell was estimated from the electron diffraction patterns to be $a = 2.7$, $b = 2.16$, $c = 0.39$ nm, in agreement with previously reported values [24–26].

At this point, it is worth noting that crystals showing the ab projection are quite unusual and when appearing present a typical square-shape morphology and very small size (< 100 nm). Most of the crystals of $Te_2M_{20}O_{57}$ grow, however, as relatively thin and long needles (> 500 nm) in the ac orientation.

Fig. 8a shows the high-resolution image corresponding to the [100] zone axis. As previously noted, the so-oriented crystals present very small particle sizes and considerable thicknesses, thus making it difficult to obtain resolved lattice images. Because of the poor quality of the image, it is difficult to distinguish the main features of the $Te_2M_{20}O_{57}$ structure. Only the contrast of the unit cell periodicity can be observed. In order to investigate the occupancy of tellurium in the 6- and 7-sided tunnels, image simulations should be performed but the poor resolution of the lattice images obtained in this projection did not allow us to compare between experimental and simulated images with success. At this point, it is important to note that Lundberg et al. did perform HREM image calculations in the isostructural cesium niobate $Cs_x(Nb,W)_5O_{14}$ [27], for different occupancy ratios showed that it was not possible to determine, from the contrast in the HREM images, whether or not some Cs ions were present in the 7-sided tunnels.

As noted above, most of the crystals of the $Te_2M_{20}O_{57}$ phase grow with the axis perpendicular to the needle-like crystal axis and, therefore, HREM images like those shown in Fig. 8b and 8c ([010] and [011] zone axes, respectively) are the most frequently found. In these unit cell projections, it is not possible to distinguish between empty and/or occupied 7-sided tunnels. Then, we assume 6-sided channels to be fully occupied and the excess of tellurium allocated in the heptagonal cavities, as previously proposed for Te- [23–26] and Sb-containing [28] MoVNbO catalysts.

The second type of crystals corresponds to the Mo_5O_{14}-type structure. The tetragonal unit cell ($a = 2.296$, $c = 0.394$ nm) can be described as a network built up by octahedral MoO_6 and MoO_7 pentagonal bipyramids mutually connected by sharing corners and edges. The pentagonal bipyramids share their edges with five MoO_6 polyhedra, forming pentagonal groups (Fig. 6b). Mo_5O_{14} tolerates the incorporation of considerable amounts of different 5 and 6 transition metals like vanadium, tungsten, niobium, and/or tantalum [29–32]. It is well known that the incorporation of these el-

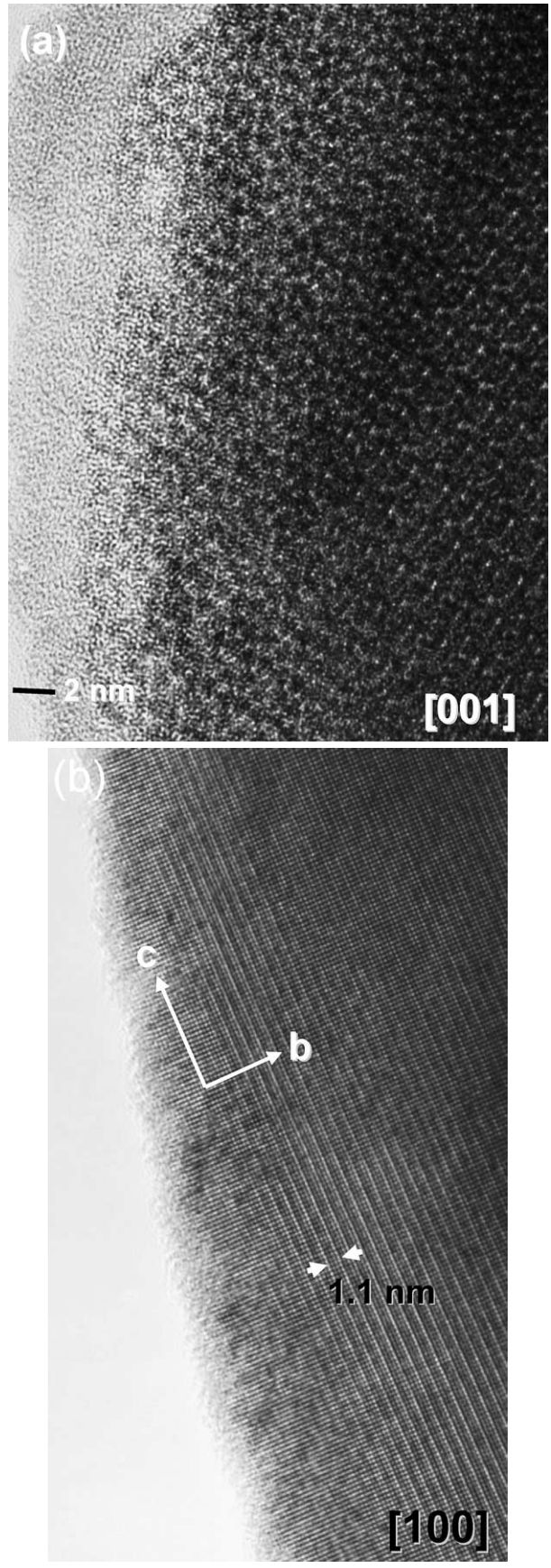

Fig. 8. HREM images of [100] (a), [010] (b), and [011] (c) zone axes of $Te_2M_{20}O_{57}$ crystal.

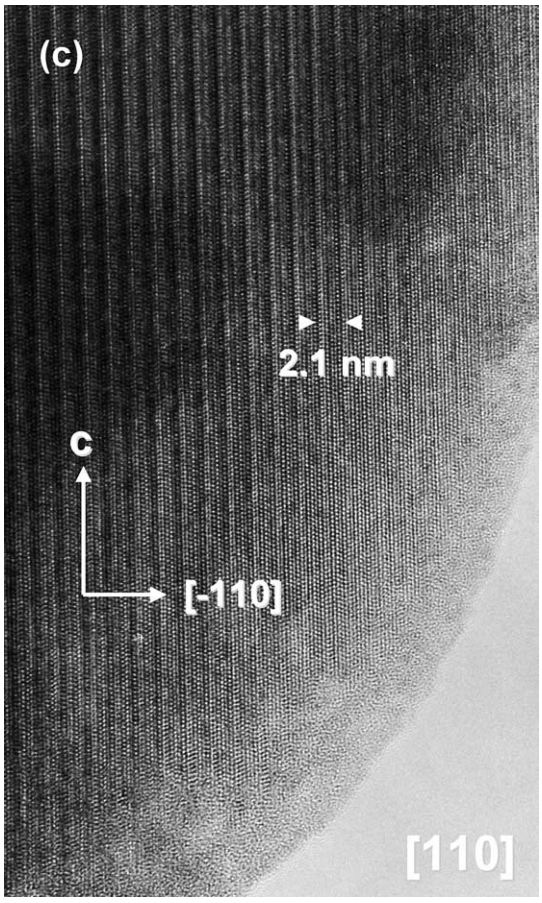

Fig. 8. (Continued).

ements leads to stabilization of the structure. Niobium and vanadium have been seen to incorporate in the Mo_5O_{14}-type structure, as revealed by EDS X-ray microanalysis. About 15–20% of molybdenum substitutes for vanadium and niobium in all the investigated crystals; vanadium and niobium relative amounts slightly vary from crystal to crystal, but the Nb/Mo ratio is always close to 0.1. The average composition corresponds to $(Mo_{0.83}Nb_{0.1}V_{0.06})_5O_{14}$.

Fig. 9a shows the SAED pattern of a Mo_5O_{14}-type crystal in the [001] reciprocal projection. The corresponding HREM image (Fig. 9b) clearly illustrates the pentagonal columns. The micrograph has been taken at a defocus value close to Scherzer condition so the black spots can be interpreted as projected columns of heavy metal atoms.

The third type of crystals corresponds to the $Te_{0.33}MO_{3.33}$ (M = Mo, V, and Nb) structure (Fig. 6c). As noted below, this phase appears only in a small quantity. EDS X-ray microanalysis showed the composition of these crystals to be very homogeneous and corresponding to the average composition $Te_{0.33}Mo_{0.7}(V,Nb)_{0.3}O_{3.33}$ in agreement with our previous data [33,34]. The microstructural details and the Te/M distribution in the unit cell of these phases have been already reported in Ref. [34].

4. Discussion

The results presented here show that MoVTeNbO mixed metal oxide catalysts are active and selective in the oxidation of ethane, as previously reported for the selective oxidation

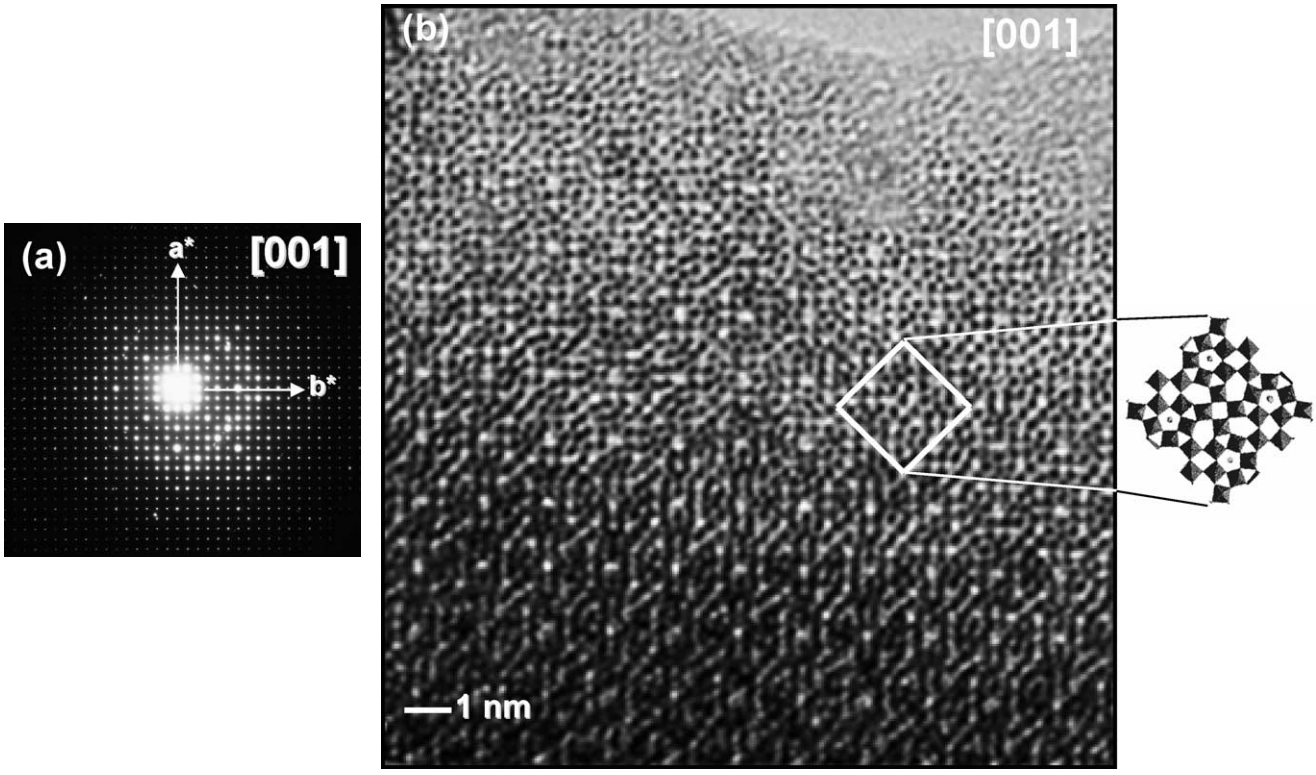

Fig. 9. (a) SAED pattern of Mo_5O_{14}-type crystal taken along [001] zone axis; (b) corresponding high-resolution micrograph.

of propane [23–26,28], although the catalytic behavior of these catalysts depends on the alkane fed. Thus, propene (at low propane conversions) and acrylic acid (at high propane conversions) are mainly observed during the oxidation of propane on MoVTeNbO catalysts [23–26,28]. However, and independently of the ethane conversion, ethylene is the main reaction product obtained during the oxidation of ethane. In addition, it must be noted that the selectivity to ethylene is higher than the selectivity to partial reaction products obtained from propane. This can be explained by considering ethylene as a relatively stable reaction product and/or a low reactivity of ethylene on these catalysts.

The fact that ethylene is only observed from ethane while partial oxygenated products are achieved from propane has also been observed in other catalytic systems. This is the case for VPO [35–38] or pyridine exchanged molybdovanadophosphoric acid [39] catalysts, in which partial oxidation products, i.e., maleic anhydride or acrylic acid, were obtained during the oxidation of *n*-butane [35,39] or propane [36,39], respectively, while ethylene was mainly obtained during the oxidation of ethane on VPO [37–39]. However, it can be noted that the selectivity to ethylene obtained on MoVTeNbO catalysts is higher than that reported previously on VPO [35–38] or pyridine-exchanged molybdovanadophosphoric acid catalysts [39]. So, the most selective MoVTeNbO catalysts present a very low reactivity in the oxidation of ethylene.

The hydrothermal synthesis of MoVTeNbO catalysts favors the formation of new crystalline phases, which are not completely observed in the corresponding ternary systems. In addition, it is clear that the composition of the catalysts determines their catalytic performance. In this way, the catalytic activity of these catalysts seems to be related to the V content of the catalyst, as previously observed during the oxidation of propane on similar catalysts [23,26]. According to this, V^{5+} species should be the active sites in alkane activation, as proposed previously by several authors in V-containing catalysts [1–7], including MoVTeNbO mixed metal oxides [23–26,28,40–43]. Although the influence of Mo species is still unclear, the presence of Mo–O–V-bridging bonds could be responsible for the high activity with respect to those observed on other V-containing catalysts. On the other hand, the role of Te could be related to both the formation of selective phases and the elimination of nonselective Mo- and V-containing crystalline phases proposed previously to be present in some MoVNb catalysts. This is the case for MoO_2, normally observed in partially reduced Mo-containing catalysts, which is active but unselective in alkane oxidation [5,12].

In addition to the chemical composition of the catalysts, the catalytic behavior of MoVTeNbO samples depends also on the calcination temperature [20]: samples calcined at low temperatures (in which amorphous material is mainly observed by XRD) present lower activity and selectivity than samples calcined in the 550–650 °C temperature range (in which crystalline phases are observed by XRD). So, it has been proposed that the ethane conversion and the selectivity to ethylene could increase with the calcination temperature in a parallel way to the formation of the main crystalline phases [20,22].

The best catalytic results reported here could be related to the presence of a $Te_2M_{20}O_{57}$ phase. However, the high yield of ethylene of the sample calcined at 650 °C cannot be directly related to the XRD results. In fact, the sample heat-treated at 650 °C (sample HT-4-B) presents a surface area lower than that heated at 600 °C (sample HT-4) and a similar XRD pattern, thus suggesting that the behavior of these catalysts could only be partially related to the nature of crystalline phases being present, which change with the calcination temperature.

Although the XRD results are not completely decisive concerning the nature of crystalline phases, SAED and HREM results confirm that the $Te_2M_{20}O_{57}$ phase is mainly observed in the most selective catalysts, although other crystalline phases, i.e., (V,Nb)-substituted θ-Mo_5O_{14} and $Te_{0.33}MO_{3.33}$ (M = Mo, V, and Nb), are also present in variable amounts.

Sample HT-4-B, heated at 650 °C, shows the same microstructural features of the corresponding catalyst calcined at 600 °C; particle size and growth orientation follow the same patterns as described before. However, big crystals (several micrometers in size) of MoO_3 are also observed, probably formed as decomposition product due to the increase in calcination temperature.

The high efficiency of MoVTeNbO catalysts in the ODH of ethane could be related to the presence of the $Te_2M_{20}O_{57}$ phase, which has also been proposed as active and selective in the partial oxidation [23–26,41,44] and the ammoxidation of propane [26,27,43]. The main structural features of $Te_2M_{20}O_{57}$, which seem to be associated with its catalytic performance, concern the pentagonal bipyramid sites (with Nb^{5+} ions preferentially located in the pentagonal sites [25,26]) and the Te-containing hexagonal tunnels.

The first characteristic is a common feature with the (V,Nb)-substituted θ-Mo_5O_{14} (see Fig. 6), whose formation is also favored in the 600–700 °C temperature range [14,29–32,45]. In the V- or Ta-substituted Mo_5O_{14}-type phases, vanadium seems to be statistically distributed [45], whereas Ta is exclusively located in the pentagonal bipyramid [31,32]. Since the pentagonal units are frequently observed as structure-building elements in niobium compounds [31], it is reasonable to think of Nb^{5+} as preferentially located in the pentagonal sites of Mo_5O_{14}, as suggested in $Te_2M_{20}O_{57}$ [26,27]. Provided this similarity between both structures it is important to note that the $Te_2M_{20}O_{57}$ phase crystallizes from a Mo–V–Te–Nb–O precursor mixture only when the Nb/V atomic ratio is 1 or higher, thus allowing us to consider the high niobium content as a possible driving force for the formation of the $Te_2M_{20}O_{57}$ orthorhombic phase [34].

Mo_5O_{14}-type oxides have been proven to be good candidates for the active and selective catalytic activity in

partial oxidation reactions. For example, V/Nb-containing Mo_5O_{14}-type oxides have been proposed as active and relatively selective in the ODH of ethane [11–14], although the presence of other crystalline aggregates, i.e., MoO_2 [11,12], can have a negative effect on the selectivity to ethylene on Te-free MoVNbO catalysts.

It has been observed that when tellurium is only incorporated on the catalyst surface, the yield of ethylene does not exceed 12% [22]. So, the catalytic results presented on Te-containing catalysts cannot be explained by the incorporation of tellurium on the catalyst surface but by the formation of active and selective Te-containing phases, i.e., $Te_2M_{20}O_{57}$, and the elimination of nonselective crystalline phases as MoO_2.

The second structural feature, i.e., the Te-containing hexagonal tunnels, is a common characteristic with the $Te_{0.33}MO_{3.33}$ (M = Mo, V, and Nb) phase. It is assumed that this phase is efficient in propene (amm)oxidation, but it is inactive in propane oxidation [46]. This crystalline phase is only present as a minor component in the most active and selective catalysts, while it is favored in sample HT-6 which presents a low catalytic activity. So, it can be concluded that the catalytic behavior of Mo–V–Te–Nb–O catalysts is mainly related to the presence of the multifunctional $Te_2M_{20}O_{57}$ orthorhombic phase in cooperation with the (V,Nb)-containing Mo_5O_{14}-type phase.

5. Conclusions

MoVTeNbO catalysts, prepared by hydrothermal synthesis, are active and highly selective in the ODH of ethane, especially those with a MoVTeNb molar ratio of 1–0.15–0.16–0.17 and heat-treated at 600–650 °C in N_2. On the best catalysts, selectivities above 80% at ethane conversion levels higher than 80% can be obtained operating at relatively low reaction temperatures (340–400 °C) and atmospheric pressure, which are the best yields reported at this moment. Therefore, a highly crystalline MoVTeNbO catalyst is an alternative way for the ethylene synthesis using a low-cost feedstock such as ethane. This behavior is different than that described during the selective propane oxidation on the same catalysts, in which acrylic acid (formed by the selective oxidation of propene) rather than propene is the main reaction product obtained at high alkane conversions. So, the good catalytic performance observed on our catalysts is due to both the high activity in the oxidative activation of ethane and the relative inactivity in ethylene oxidation.

$Te_2M_{20}O_{57}$ (M = Mo, V, and Nb) and (V,Nb)-substituted θ-Mo_5O_{14}, in addition to small amounts of the $Te_{0.33}MO_{3.33}$ (M = Mo, V, and Nb) phase, can be proposed in the most selective catalysts from XRD, SAED, and HREM results, although the catalytic performance in ethane oxidation can be related to the presence of the multifunctional $Te_2M_{20}O_{57}$ orthorhombic phase in cooperation with the Mo_5O_{14}-type phase, which is selectively formed by using hydrothermal synthesis. The appearance of the $Te_{0.33}MO_{3.33}$ (M = Mo, V, and Nb) phase could favor a lower catalytic activity in ethane conversion, in the same way as that proposed in the selective oxidation of propane.

Acknowledgment

Financial support from DGICYT in Spain through Projects PPQ2003-03946 and MAT2001-1440 is gratefully acknowledged.

References

[1] S. Alboneti, F. Cavani, F. Trifiró, Catal. Rev.-Sci. Eng. 38 (1996) 413.
[2] M.M. Bettahar, G. Costentin, L. Savary, J.C. Lavalley, Appl. Catal. A 145 (1996) 1.
[3] R.K. Grasselli, Top. Catal. 15 (2001) 93.
[4] H.H. Kung, Adv. Catal. 40 (1994) 1.
[5] F. Cavani, F. Trifiró, Catal. Today 24 (1995) 307.
[6] T. Blasco, J.M. López Nieto, Appl. Catal. A 157 (1997) 117.
[7] M. Bañares, Catal. Today 51 (1999) 319.
[8] E. Morales, J.H. Lunsford, J. Catal. 118 (1989) 255.
[9] J.M. López Nieto, Top. Catal. 15 (2001) 189.
[10] E.M. Thorsteinson, T.P. Wilson, F.G. Young, P.H. Kasai, J. Catal. 52 (1978) 116.
[11] (a) M. Merzouki, B. Taouk, L. Monceaux, E. Bordes, P. Courtine, Stud. Surf. Sci. Catal. 72 (1992) 165;
(b) K. Ruth, R. Kieffer, R. Burch, J. Catal. 175 (1998) 16.
[12] D. Linke, D. Wolf, M. Baerns, O. Timpe, R. Schogl, S. Zeyß, U. Dingerdissen, J. Catal. 205 (2002) 16.
[13] W. Ueda, K. Oshihara, Appl. Catal. A 200 (2000) 135.
[14] P. Botella, J.M. López Nieto, A. Dejoz, M.I. Vázquez, A. Martínez-Arias, Catal. Today 78 (2003) 507.
[15] Y. Liu, P. Cong, R.D. Doolen, S. Guan, V. Markov, L. Woo, S. Zeyss, U. Dingerdissen, Appl. Catal. A 254 (2003) 59.
[16] T. Johann, A. Brenner, M. Schwickardi, O. Busch, F. Marlow, S. Schunk, F. Schuth, Catal. Today 81 (2003) 449.
[17] G. Grubert, E. Kondratenko, S. Kolf, M. Baerns, P. van Geem, R. Parton, Catal. Today 81 (2003) 337.
[18] F.G. Young, E.M. Thorsteinson, US patent 4,250,346, 1983.
[19] J.H. McCain, US patent 4,524,236, 1985.
[20] J.M. López Nieto, P. Botella, M.I. Vázquez, A. Dejoz, Chem. Commun. (2002) 1906.
[21] J.M. López Nieto, P. Botella, M.I. Vázquez, A. Dejoz, WO patent 03/064035, 2003.
[22] J.M. López Nieto, P. Botella, P. Concepción, A. Dejoz, M.I. Vázquez, Catal. Today (2004), in press.
[23] P. Botella, J.M. López Nieto, B. Solsona, A. Mifsud, F. Márquez, J. Catal. 209 (2002) 445.
[24] J.M.M. Millet, H. Roussel, A. Pigamo, J.L. Dubois, J.C. Dumas, Appl. Catal. A 232 (2002) 77.
[25] P. DeSanto, D.J. Buttrey, R.K. Grasselli, C.G. Lugmair, A.F. Volpe, B.H. Toby, T. Vogt, Top. Catal. 23 (2003) 23.
[26] R.K. Grasselli, J.D. Burrington, D.J. Buttrey, P. DeSanto, C.G. Lugmair, A.F. Volpe, T. Weingand, Top. Catal. 23 (2003) 5.
[27] M. Lundberg, M. Sundberg, Ultramicroscopy 52 (1993) 429.
[28] J.M.M. Millet, M. Baca, A. Pigamo, D. Vitry, W. Ueda, J.L. Dubois, Appl. Catal. A 244 (2003) 359.
[29] J. Tichý, Appl. Catal. A 157 (1999) 363.
[30] T. Ilkenhans, B. Herzog, T. Braun, R. Schlögl, J. Catal. 153 (1995) 275.
[31] T. Ekström, M. Nygren, Acta Chem. Scand. 26 (1972) 1836.
[32] N. Yamazoe, L. Kihlborg, Acta Crystallogr. B 31 (1975) 1666.

[33] E. García-González, J.M. López Nieto, P. Botella, J.M. González-Calbet, Chem. Mater. 14 (2002) 4416.
[34] E. García-González, J.M. López Nieto, P. Botella, B. Solsona, J.M. González-Calbet, Mater. Res. Soc. Symp. Proc. 755 (2003) 327.
[35] F. Cavani, F. Trifiró, Catal. Today 51 (1999) 561.
[36] G. Landi, L. Lisi, J.C. Volta, Chem. Commun. (2003) 492.
[37] P. Michalakos, M.C. Kung, I. Jahan, H.H. Kung, J. Catal. 140 (1993) 226.
[38] B. Solsona, V.A. Zazhigalov, J.M. López Nieto, I.V. Bacherikova, E.A. Diyuk, Appl. Catal. A 249 (2003) 81.
[39] J.H. Holles, C.J. Dillon, J.A. Labinger, M.E. Davis, J. Catal. 218 (2003) 42.
[40] P. Botella, B. Solsona, A. Martinez-Arias, J.M. López Nieto, Catal. Lett. 74 (2001) 149.
[41] R.K. Grasselli, in: J. Bonelle, B. Delmon, E. Derouane (Eds.), Surface Properties and Catalysis by Non-Metals, Reidel, Dordrecht, 1983, p. 273.
[42] R.K. Grasselli, in: G. Ertl, H. Knözinger, J. Weitkamp (Eds.), in: Handbook of Heterogeneous Catalysis, vol. 5, VCH, Weinheim, 1997, p. 2303.
[43] J. Holmberg, R.K. Grasselli, A. Anderson, Top. Catal. 23 (2003) 55.
[44] D. Vitry, Y. Morikawa, J.L. Dubois, W. Ueda, Appl. Catal. A 251 (2003) 411.
[45] L. Kihlborg, Acta Chem. Scand. 23 (1969) 1834.
[46] P. Botella, J.M. López Nieto, B. Solsona, Catal. Lett. 78 (2002) 383.